# Analysis of confined spray processes for powder production

A. Lampa*, U. Fritsching
Particle and Process Engineering, University of Bremen, Germany
lampa@iwt.uni-bremen.de and ufri@iwt.uni-bremen.de

**Abstract**

The tailoring of the particle and powder properties that are produced within spray processes is influenced by various unsteady transport processes in the dispersed multiphase spray flow in a confined spray chamber. In this context differently scaled spray structures in a confined spray environment have been analyzed experimentally and numerically. The basic setup of the study consists of a twin-fluid atomizer central top-spraying in a confined spray chamber, where the atomizer gas can be heated up to 500°C. Mixing phenomena of momentum, energy and species play an even bigger role for this hot-gas atomization and drying process than in a conventional tall form spray dryer. The experimental investigations have been carried out with Particle-Image-Velocimetry to determine the kinetic data of the gas and the discrete phase. Additionally Large-Eddy-Simulations have been set up to predict the transient behaviour of the process and give more insight into the sensitivity of the droplet-gas interactions in dependency to the spray chamber design.

## Introduction

For spray processes including mass transfer between droplets and gas, the spray experiences an intense contact with the drying medium. During this contact, droplets usually meet hot air in the spraying chamber. The large surface area of the droplets leads to rapid evaporation rates, keeping the temperature of the droplets at the wet-bulb temperature. During spray drying the particle behaviour is dependent on the air flow pattern. Coherent gas flow patterns in the near nozzle-area are strongly interacting with the droplet collectives. Unsteady recirculation and entrainment flow patterns are effected by the spray chamber design [1]. The instability of the spray flow is promoted by these perturbations. The result is a preferential concentration of the droplets within the spray, thus altering the drying kinetics for individual droplets within the drying process. The effect of spray chamber design and nozzle parameters on the clustering of droplets in the sprays of twin-fluid atomizers has been analyzed in [2], [3]. Coherent gas flow patterns in the near nozzle-area are strongly interacting with the droplet collectives. Unsteady recirculation and entrainment flow patterns are effected by the spray chamber design [1]. The instability of the spray flow is promoted by these perturbations. The result is a preferential concentration of the droplets within the spray, thus altering the drying kinetics for individual droplets within the drying process.

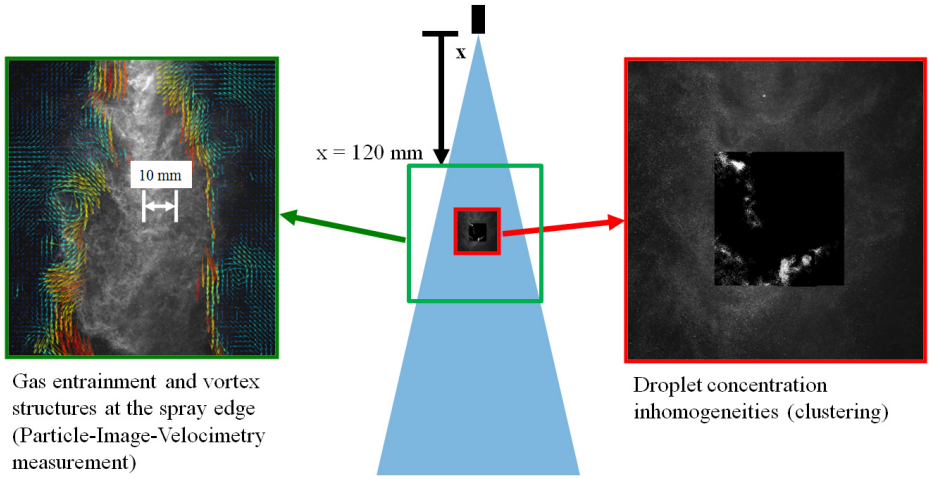


**Figure 1** Coherent gas flow structures in the near nozzle region of the spray in a twin-fluid atomizer and droplet cluster formation (Particle-Image-Velocimetry measurements)

In Figure 1 the coherent gas flow structures at the edge of the spray cone of an external mixing twin-fluid atomizer are depicted. Clustering of droplets can be observed within the spray. The effect of spray chamber design and nozzle parameters on the clustering of droplets in the sprays of twin-fluid atomizers has been analyzed

* Corresponding author: lampa@iwt.uni-bremen.de

in [2]. Squires and Eaton [4] found that in dispersed two-phase flows the particles/droplets preferrentially accumulate in areas of high strain and low vorticity. Especially when the Stokes number of the droplets/particles is close to unity clustering can be observed. The Stokes number for spherical droplets is defined as follows:

$$St_{droplet} = \frac{\rho_{droplet} \cdot d_{droplet}^2 \cdot u_{rel}}{18 \cdot \eta_{gas} \cdot L_{ref}} \quad (1)$$

$\rho_{droplet}$ is the density of the droplet and $d_{droplet}$ is the droplet diameter. $u_{rel}$ is the relative velocity between droplet and gas. $\eta_{gas}$ is the dynamic viscosity of the gas. The reference length $L_{ref}$ is a characteristic scale of the gas motion. The value of this scale depends on the location of the droplets in the gas flow. For the drag coefficient Stokes law is assumed to be valid.

Beside the heat and mass transfer also the tendency for the droplets/particles to collide and agglomerate is influenced by the clustering and the local gas flow patterns. Technical jets and sprays with pneumatic energy support are usually characterized by high gas Reynolds numbers, which require advanced turbulence modelling due to limited computational ressources. In this paper the effect of spray parameters on the large-scale fluctuation of gas and droplets will be investigated experimentally and numerically. Numerically the fluctuating scales have been resolved with Large-Eddy-Simulation (LES) [5]. Special attention has to be drawn on the initiation of the turbulence structures at the inflow of the domain (see e.g. [6]) . In the experimental part twin-fluid nozzles in a confined environment have been analyzed with planar Particle-Image-Velocimetry to yield the kinetic data of droplets and gas (cf. [2]).

**Experimental and Numerical Methods**

Three different conically shaped spray chambers have been analysed (Fig. 2, V1-V3). The cross sections are quadratic with different sized starting cross sections. The expansion angle of the conical spray chambers is varied. The spray is removed from the chamber through an iso-kinetic vacuum-outlet. The setup consist of a center top-spraying atomizer nozzle operated at a volumetric gas flow rate of 52 l/min (0.0624 kg/min) and a water mass flow of 0.1 kg/min. The atomizer type is a twin-fluid external mixing close-coupled atomizer (Fig. 3 left). The spray angle at an absolute atomizer gas pressure of 5 bar is about 18°.

For analysis of the spray structure, a dual-cavity Nd:YAG laser (65 mJ /pulse at 532 nm) is used to illuminate the spray within the center plane of the spray plume (Fig. 2). The CCD-camera optical axis is perpendicular to the laser light sheet plane. The camera records the scattered light of the droplets with a 12-bit image sensor with 2048 x 2048 pixels. The distance between the camera and the light sheet is varied, such that the resulting window size ranges from 57 mm x 57 mm (36.0 pixels/mm) for the tracking of the droplets within the spray cone to 232 mm x 232 mm (13.1 pixels/mm) for the analysis of the recirculation patterns of the gas. The camera has a maximum sampling frequency of 7 Hz collecting 1000 double frames for each setting.

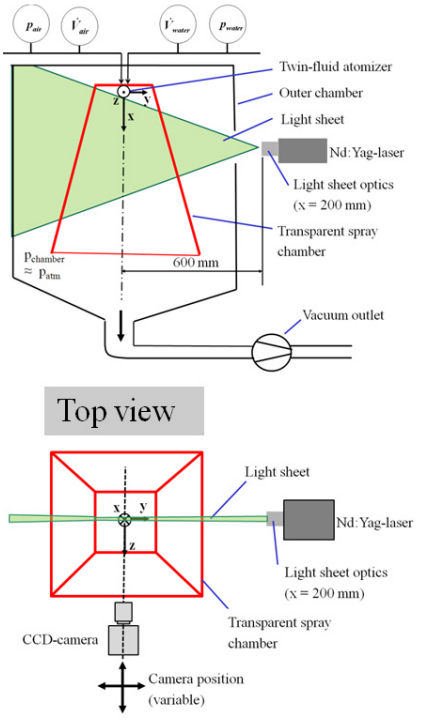


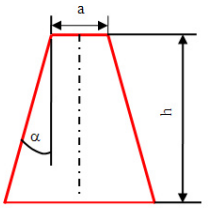


| Variant | a [mm] | α [°] | h [mm] | B [mm] |
|---|---|---|---|---|
| V1 | 200 | 10 | 900 | 517 |
| V2 | 200 | 15 | 900 | 682 |
| V3 | 400 | 0 | 900 | 717 |

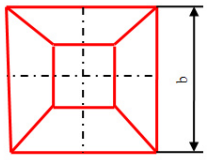


**Figure 2** Experimental setup (PIV) and differently shaped spray chamber geometries

The spray produced by the external-mixing atomizer yields a median droplet size $d_{50,3}$ of 30µm. The droplet size distribution was measured with laser diffraction measurements (Fig. 3 right). Droplet collectives show a characteristic concentration pattern ("fir tree" pattern [3], Fig. 3 left) beginning at the nozzle exit und propagating downstream.

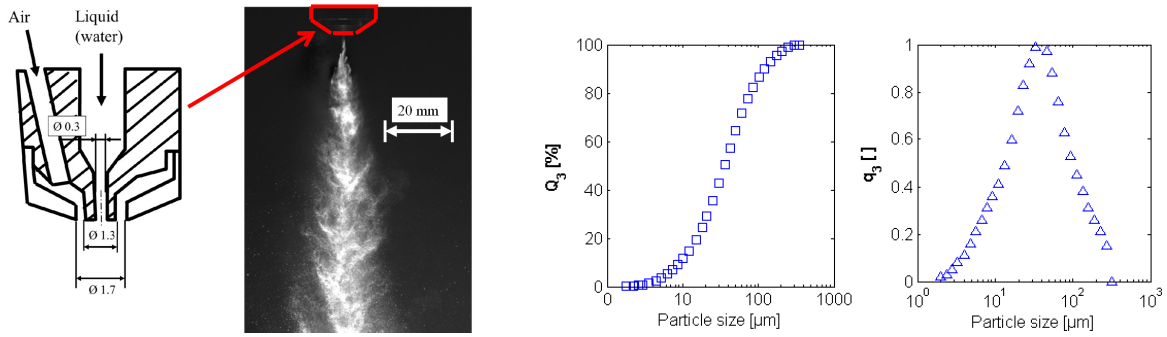


**Figure 3** Nozzle geometry and characteristic spray pattern (left) and corresponding droplet size distribution at $p_{abs}$= 5bar (right)

For the simulation (Fig. 4) of the gas flow structures the Dynamic Smagorinsky Large-Eddy-Simulation (LES) turbulence model has been applied. The flow has been calculated incompressible. Compressibility effects near the nozzle are not regarded. The water droplet trajectories have been calculated with a 2-way coupling lagrangian particle tracking algorithm. For a statistic representation and realistic coupling with the gas phase the parcel injection rate must be set to a minimum rate of 180 parcels per µs. The minimum number of parcels for evaluating droplet cluster phenomena in this setup is 1 million.

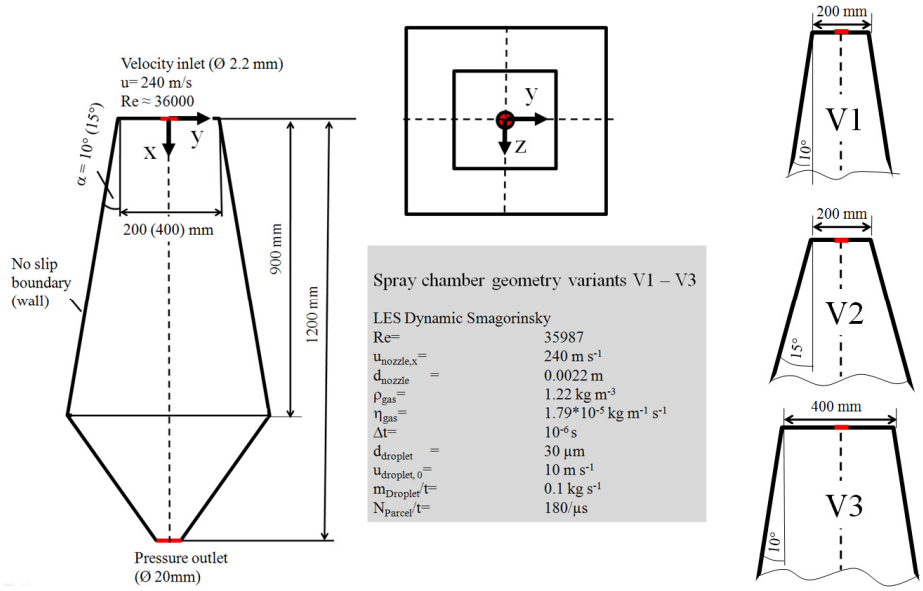


**Figure 4** Numerical setup for 3 different spray chamber geometries (V1-V3)

The aim of the simulation is to analyze the effects of mixing and entrainment near the nozzle (0 < x < 300 mm) and its effect on the clustering of droplets. The mesh (Fig. 5) consists of two concentric O-grids. At the top the inner O-grid has a diameter 2.2 mm corresponding with the inlet diameter. It is expanding in the streamwise direction to a square shape with the side lengh 50 mm at z= 900 mm. The mesh consists of about 2.8 $10^6$ cells for the case with lagrangian particle tracking. In this numerical setup also the droplet clustering can be investigated. For the geometry sensitivity study (single phase gas flow, 3 cases: V1-V3) the mesh consists of about 1.5 $10^6$ cells. The maximum resolution near the nozzle is 24 cells/mm. The motion of the continuous phase has been initialized with a steady-state k-ω-SST turbulence model.

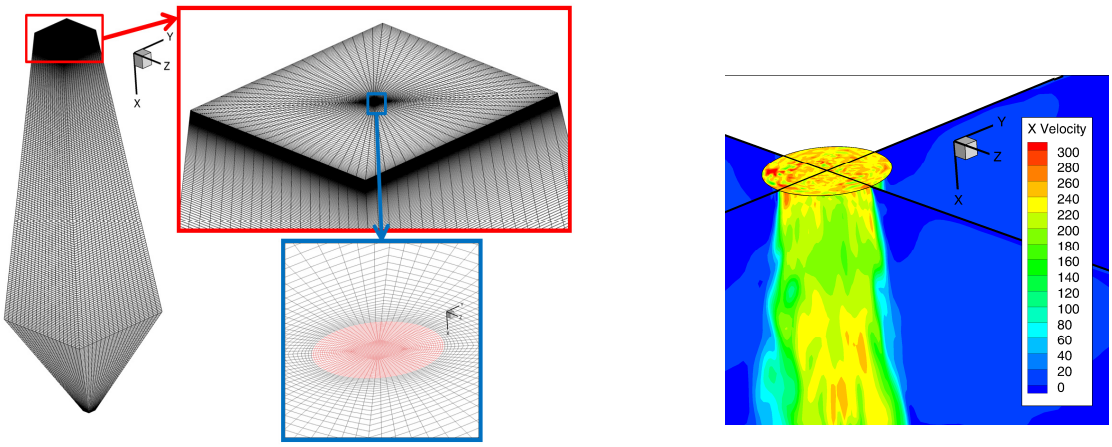


**Figure 5** Mesh for LES (left) and synthetic gas flow perturbation at the inlet (right), LES, $u_{inlet,\,x}$ =240 m/s, Tu= 20%, $\Delta t = 10^{-6}$ s

The turbulent perturbations at the inlet (Fig. 5 left) are being generated by the vortex method ([7], [8]). The vortex method is a time-dependent inlet condition, creating perturbations added on a specified mean velocity profile via a fluctuating vorticity field (i.e. two-dimensional in the plane normal to the streamwise direction). The vortex method is based on the Lagrangian form of the 2D evolution equation of the vorticity and the Biot-Savart law. A particle discretization is applied to solve this equation. These particles, or "vortex points" are convected randomly and carry information about the vorticity field. A Detached-Eddy-Simulation (DES) turbulence model may not be used in the context of this numerical setup, because perturbations generated at the inlet are suppressed (cf. [9]). Also the cell size needs to be small in this particular area to resolve the fluctuations propagating from the inlet.

**Results and Discussion**

In the spray zone close to the outer edge of the spray where large velocity gradients and thus high shear rates are to be found, complex interactions between gas and droplets take place. A characteristic flapping of the jet in combination with a precession movement of the spray plume can be seen in the numerical simulation and also in the experiment. For partly responsive droplets within the spray cone ($d_{droplet}$= 30 µm, $St_{droplet} \approx 1$: 200 mm < x <300 mm) droplet concentration inhomogeneities are forming (Fig. 6).

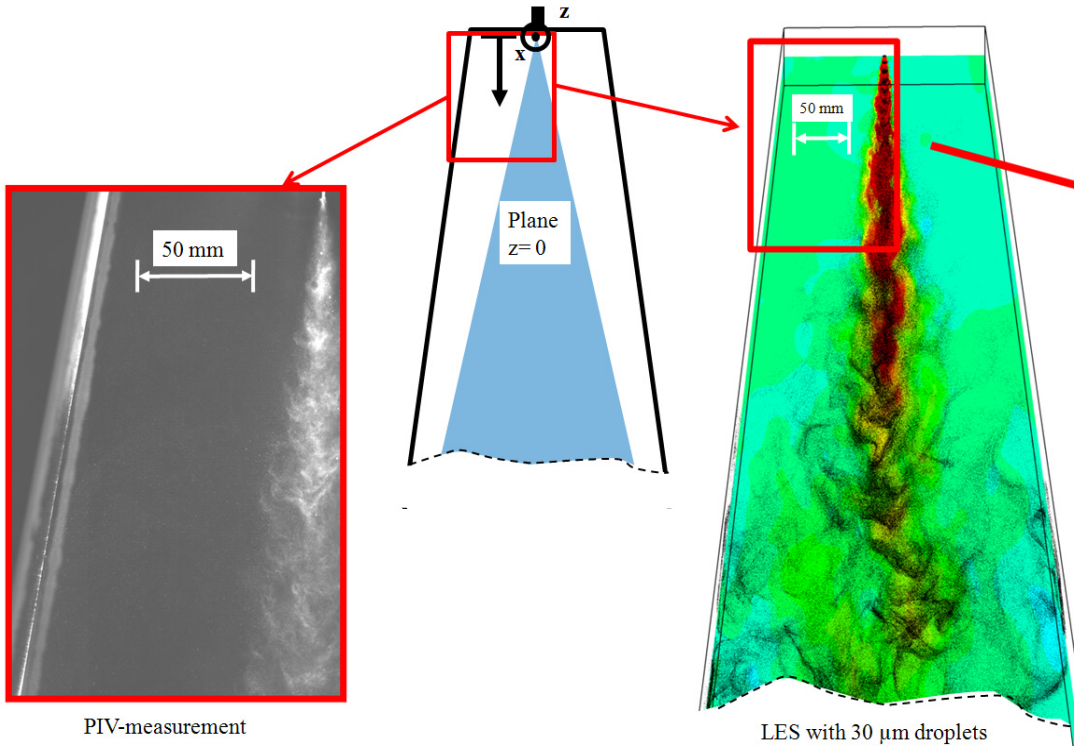


**Figure 6** Spray pattern and droplet clustering
(left) PIV measurements (variant V1, $p_{abs}$= 5bar) (right) LES, 30µm droplets (variant V1)

The characteristic spray flow pattern from the experiments can be reproduced. The first stage of droplet mixing with the air takes place until 50 mm from the nozzle, where the planar injection pattern is changing into randomly distributed droplet pattern. Further down the characteristic fir tree pattern is formed. In the experiment the droplet clustering pattern are to be seen directly after the nozzle exit (Fig. 3), whereas the droplet clustering in the numerical simulation with single sized droplets is seen at a distance x > 150 mm. The reason for this effect is that the inertial moment of the big droplets is high enough not to interact strongly with the gas phase ($St_p$>>1). Smaller droplets, which have a lower initial momentum, strongly interact with the vortex and entrainment structures at the spray cone edge ($St_p$≈ 1).

For the validation of the LES spray simulation the numerical results have been compared with PIV-measurements in the range 100-170 mm in the streamwise direction. Generally the PIV-method is more sensitive to larger droplets due to their stronger light scattering signal [10]. Thus a comparison with the numerical simulation with 30 µm droplets is given. The axial velocity for the droplets on the spray axis shows in principle good agreement with the measured data (Fig. 9). Generally the mean absolute droplet velocity is higher than the mean absolute gas velocity in this region of the spray. The standard deviation of the axial velocity component is indicated. The decay of the fluctuation movement of the droplets with larger distance to the nozzle can also be well predicted.

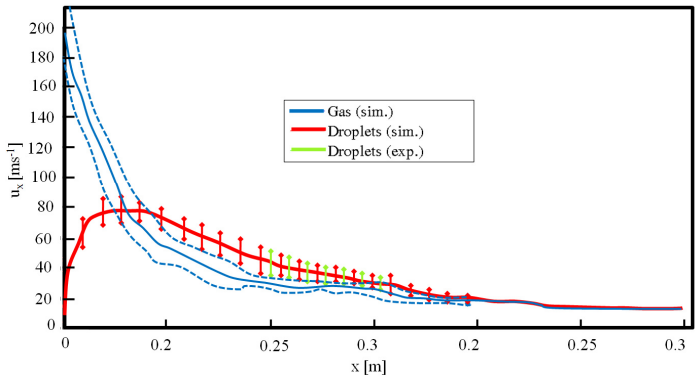


**Figure 7** Axial gas and droplet velocity on spray axis (LES) and validation with experimental droplet velocity (PIV, $p_{abs}$= 5 bar)

For the radial distribution of the axial velocity component (Fig. 11) a marginally lower amplitude of the axial velocities for the numerical simulations can be observed. Also the standard deviation of the fluctuating axial velocity component is predicted lower. But still the simulated results lie well within the standard deviation of the experimental data.

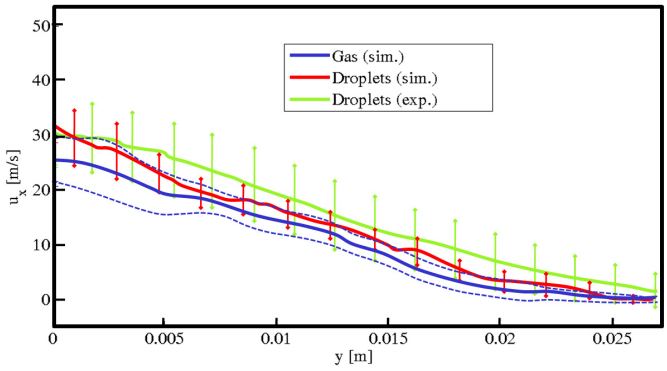


**Figure 8** Validation of simulated axial gas and droplet velocity in radial direction at x = 150 mm

Droplet clustering may originate from the disintegration process where ligaments break up into a cloud of smaller droplets [3]. Also droplet clustering may occur when large scale turbulent / coherent flow structures interact with the droplets. For the influence of small scale turbulence it has been found, that particle tend to have a preferential concentration in the gas phase in regions with a high strain rate and low vorticity [4], [11] and low turbulence intensity [12]. In the investigated case (Fig. 12) the interaction of the droplets with turbulent coherent gas structures is the most important phenomenon. Centrifuging of droplets/particles is only likely in the vicinity of vortices. The large scale vortices are located at the edge of the spray cone flow. Small scale vortices cannot be

detected by the PIV-measurements in the current setup because of the limited spatial resolution. This resolution is dependent on the measurement window (36.0 pixels/mm) to track the droplet clusters where the mean cluster scale is in the order of 10 mm [2].

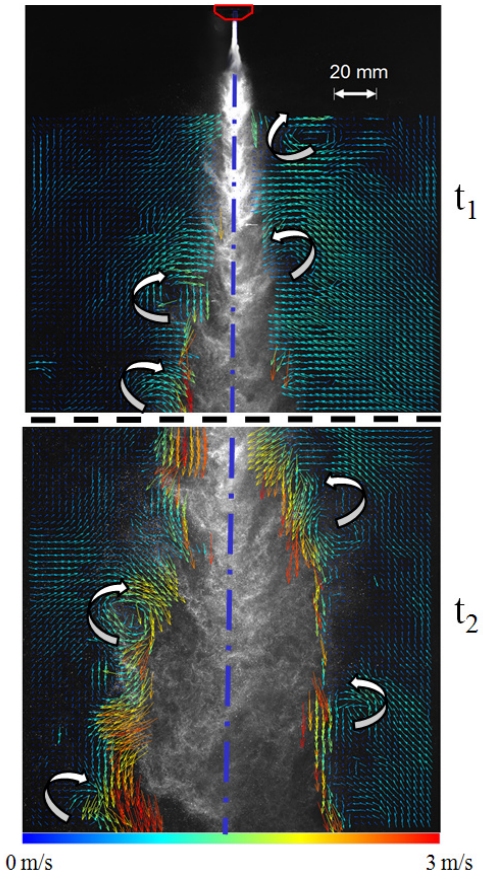


**Figure 9** Gas vortices at the edge of the spray cone, $p_{abs}$= 5bar (tracer-PIV measurements, 2 inst. Pictures $t_1$: x=0 – 170 mm, $t_2$: x= 170 – 340 mm)

The spray flow itself is strongly influenced by the local entrainment of gas. The entrainment is strongest upstream the center of the vortices at the spray edge. Gas, loaded with a low mass fraction of droplets, is entrained into the the spray cone flow and reduces the gas and droplet axial velocity in the spray flow. Gas and droplets with a higher velocity upstream are diverted and the strain within the gas phase is increased. This is one possible explanation how the spray jet is segmented and droplets show a preferential concentration, respectively clustering. For the PIV-measurements in the current setup it is not possible to determine gas and droplet velocities simultaneously (2 phase-PIV, [13], [14]).

The results of the LES simulation provide full access to droplet-air interactions within the spray cone flow. For the LES simulation a rectangular zone (x-y-z: 100 mm x 100 mm x 5 mm) in the center of the spray starting at x = 200 has been extracted (Fig. 10). Droplet clustering occurs especially in the center of the spray. The blue vectors depict the droplet's (parcel's) velocity in the x-z plane, while the red vectors indicate the gas velocites in the x-z plane. The droplet velocity does not differ much from the ambient gas velocity (see also Fig. 7 and Fig. 8). High concentrations of droplets can be found especially in regions of the gas flow, whereas no (large scale) vortices can be found within the spray.

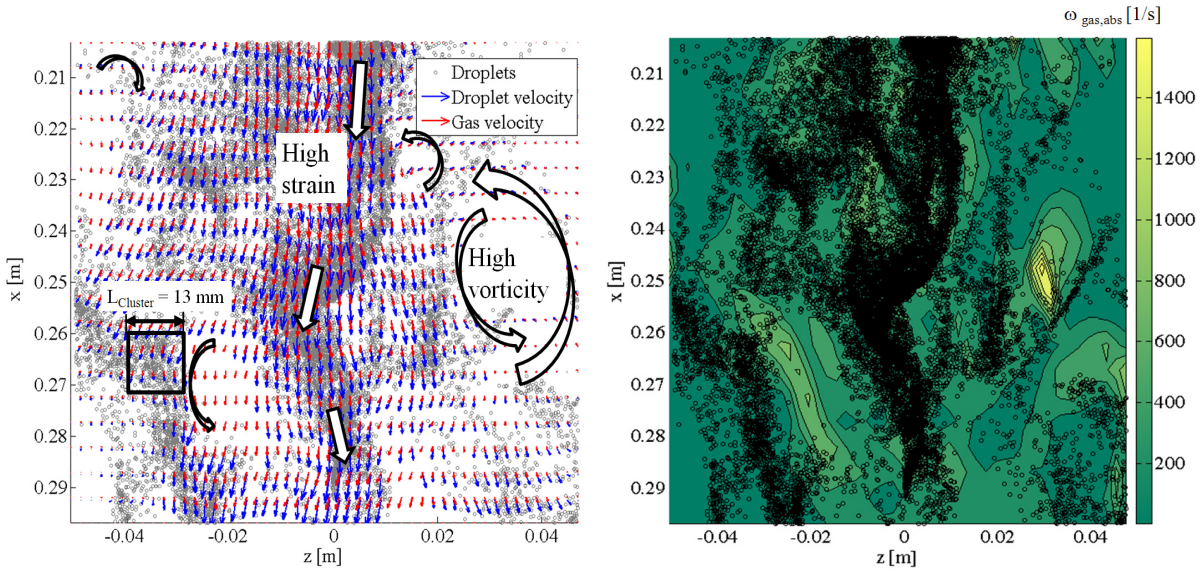


**Figure 10** Gas and droplet velocities (left) within the spray, droplet clustering and instantaneous vorticity field (right), LES simulation

To quantify the droplet-gas interactions correlations between the number of parcels and the flow quantities have been evaluated. The spatially integrated correlation coefficient for a single time step is defined as follows:

$$r_{A,B} = \frac{\sum_m \sum_n (A_{mn} - \overline{A})(B_{mn} - \overline{B})}{\sqrt{(\sum_m \sum_n (A_{mn} - A)^2)(\sum_m \sum_n (B_{mn} - \overline{B})^2)}} \quad (2)$$

, whereas $A_{mn}$ , $B_{mn}$ depict the spatially resolved and $\overline{A}$, $\overline{B}$ the spatially integrated scalar quantities. For the evaluations the number of droplets per volume have been correlated with different scalar quantities like the value of the normalized probability density function of the Stokes number at St = 1.

Tabel 1: Spatially integrated correlation coefficients

| $r_{\text{number parcel, PDF(St =1)}}$ | $r_{\text{number parcel, 1/\|ω (vorticity)\|}}$ | $r_{\text{number parcel, \|S(strain, x-direction)\|}}$ |
|---|---|---|
| 0.85 | 0.90 | 0.73 |

It shows that after investigating the mean correlation coefficients of 100 uncorrelated time steps clustering takes place in areas of the flow, where the Stokes number is close to unity. Also the clusters tend to be in areas of low vorticity. For the strain it has to be stated that only the axial component correlates weakly with the number of parcels. This might be due to the fact, that the flow is strongly anisotropic (cf. [4]).

The influence of the spray chamber design on the clustering of droplets has been experimentally analyzed in [2]. The result is that the overall spray structures do not change significantly for the different spray chamber designs. The measured parameter is the integral cluster scale (Garncarek algorithm, [15]). The box-counting algorithm has been used to determine the cluster size for a single LES case (variant V1). It has been found that the average cluster scale is 13 mm (+- 4 mm standard deviation). In [2] the median of the integral cluster scale has been found as 12 mm +- 3 mm standard deviation. If the unsteady entrainment is responsible for the segmentation of the spray jet and the formation of droplet clusters, the entrainment flow structures should be similar for all geometric variants. Figure 11 depicts the x-velocity component of the gas on the spray axis. The median as well as the standard deviation for all 3 variants show a good agreement in regions where clustering of droplets takes place (150 < x < 300 mm).

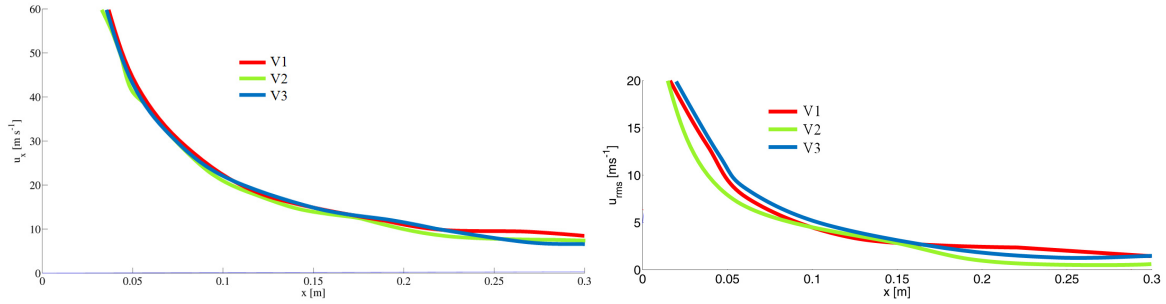


**Figure 11** Mean (left) and RMS-Values (right) of axial gas velocity on the spray axis for different spray chamber geometries

The entrainment for the different chamber geometries V1-V3 is characterized by the unsteady entrainment and vortex formation at the spray edge (Fig. 12). The absolut gas velocity outside the spray or close to the spray edge is affected by the spray chamber design (cf. [2]). The flow structures outside the spray cone flow induce the integral entrainment of air which is responsible for the heat and mass transfer and thus for the drying kinetics of the droplets. Despite of this the local entrainment patterns of air look very similar. Perturbation created at the inlet need time to permeate through the domain and are able to influence the recirculation movement. RANS-turbulence models tend to dampen these fluctuations whereas LES-modells can, in dependency of the mesh, time step, etc. promote these instabilities and may lead to unrealistic flow phenomena, especially in the beginning of the simulation.

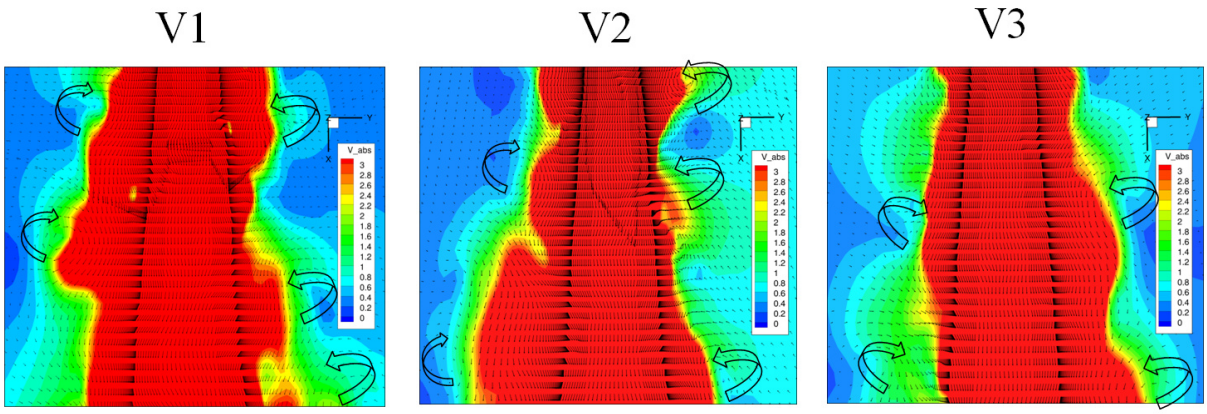


**Figure 12** Unsteady entrainment patterns at the spray edge for different geometry cases for x= 120-220mm (LES simulation)

Nevertheless the spray cone flow near the nozzle is only scarcely affected by this phenomenum. Future LES-simulations focus on the spray flow pattern, especially the droplet clustering, in regions close to the nozzle. The stability of the spray jet has to be analyzed in dependence of the turbulence model, boundary conditions, etc in more detail. Generally the different time and length scales in sprays make it difficult to apply a universal turbulence model. The time to reach a reasonable convergence of the flow for the LES setup presented in this paper can be considerably high ($t > 1s$, $\Delta t = 10^{-6}$). In addition, the sampling frequency of data outside the spray flow must be rather low (e.g. 10 samples/ s). When performing an integral spray process simulation, the switching between RANS and LES models may be necessary.

## Summary and Conclusions

The application of Large-Eddy-Simulation (LES) in the analysis of bounded spray processes in enclosures has been shown. The simulations of the droplet-air interactions showed good agreement with PIV-measurements within the spray. Also the clustering behaviour of droplets in the spray could be predicted according to findings in the literature. The initiation of the spray flow and the boundary conditions play a crucial role for the realistic simulation of the spray flow. For practical design of the spray process the initiation of the spray flow and the data sampling require special attention and computational resources. LES spray simulations gain a much better insight in the droplet-gas interactions and the unsteady spray flow pattern. For the clustering of droplets within the spray, it could be shown that the complex interactions within the shear layer are the driving force for the formation of droplet clusters. The transient entrainment of air into the spray promotes the segmentation of the jet, while the large scale vortex patterns do not directly interact with the inner spray flow. The influence of the spray chamber design on the spray behaviour and therefore on the clustering of droplets in the near field of the nozzle is low. Special care has to be taken when strong recirculations of the gas flow take place. The unsteadiness and slow temporal evolution of the recirculating flow pattern make it difficult and time-consuming to compute such flows. In future works an advanced 3D-tracking of clusters may be performed to depict the different ambient conditions individual droplets/particles experience in the gas flow and its impact on heat and mass transfer processes. In addition, a multiscale process model for the application in industrial scale spray processes for powder production will be developed.

## Acknowledgements

This work has been performed within the project SPP 1423 Process Spray funded by the Deutsche Forschungsgemeinschaft (DFG). The support from the DFG is gratefully acknowledged.

## References

[1] Scholler, M. and F. U., *InternationalJournal of Flow Control*, **1**(2): p. 167-173 (2009)
[2] Lampa, A. and U. Fritsching, *Atomization and Sprays*, **21**(9): p. 737–752 (2011)
[3] Heinlein, J. and U. Fritsching, *Experiments in Fluids*, 2006. **40**(3): p. 464-472.
[4] Eaton, J.K. and J.R. Fessler, *International Journal of Multiphase Flow*, **20**(Supplement 1): p. 169-209 (1994)
[5] Bouffanais, R., *Computers & Fluids*, **39**(5): p. 735-738 (2010)
[6] Kempf, A., M. Klein, and J. Janicka, *Flow, Turbulence and Combustion*, **74**(1): p. 67-84 (2005)
[7] Ansys Inc, *Ansys Fluent 13.0.0 Manual* (2011)
[8] Mathey, F., et al., *Turb. Heat Mass Transfer*, **4**. (2003)
[9] Peng, S.-H. and W. Haase, *Advances in Hybrid RANS- LES Modelling 2008*, Springer. p. 97-106 (2009)

[10] Raffel, M., et al., *Particle Image Velocimetry - A Practical Guide*, Springer: Berlin, Heidelberg (2009)
[11] Li, D., et al., *International Journal of Multiphase Flow*, **37**(6): p. 539-554 (2011)
[12] Longmire, E.K. and J.K. Eaton, *Journal of Fluid Mechanics* **236**: p. 217-257 (1992)
[13] Hardalupas, Y., et al., *Experiments in Fluids*, **49**(2): p. 417-434 (2010)
[14] Rottenkolber, G., *Forschungsberichte aus dem Institut für Thermische Strömungsmaschinen.* Vol. Bd. 14/2001, KIT: Karlsruhe. 175 (2001)
[15] Czainski, Garncarek, and Piasecki, *Journal of Physics D: Applied Physics*, **27**: p. 612-622 (1993)